Open access • Journal Article • DOI:10.1140/EPJB/E2009-00001-3

Nonlinear voter models: the transition from invasion to coexistence

Frank Schweitzer, Laxmidhar Behera

Institutions: ETH Zurich, Indian Institute of Technology Kanpur

Published on: 13 Jan 2009 - European Physical Journal B (Springer)

Topics: Nonlinear system

Nonlinear voter models

The transition from invasion to coexistence

Eur. Phys. J. B **67**, 301–318 (2009)
DOI: 10.1140/epjb/e2009-00001-3

THE EUROPEAN PHYSICAL JOURNAL B

Regular Article

Nonlinear voter models: the transition from invasion to coexistence

F. Schweitzer[1,a] and L. Behera[2]

[1] Chair of Systems Design, ETH Zurich, Kreuzplatz 5, 8032 Zurich, Switzerland
[2] Department of Electrical Engineering, Indian Institute of Technology, Kanpur 208 016, India

Received 24 August 2008 / Received in final form 8 December 2008
Published online 13 January 2009 –

Abstract. In nonlinear voter models the transitions between two states depend in a nonlinear manner on the frequencies of these states in the neighborhood. We investigate the role of these nonlinearities on the global outcome of the dynamics for a homogeneous network where each node is connected to $m = 4$ neighbors. The paper unfolds in two directions. We first develop a general stochastic framework for frequency dependent processes from which we derive the macroscopic dynamics for key variables, such as global frequencies and correlations. Explicit expressions for both the mean-field limit and the pair approximation are obtained. We then apply these equations to determine a phase diagram in the parameter space that distinguishes between different dynamic regimes. The pair approximation allows us to identify three regimes for nonlinear voter models: (i) complete invasion; (ii) random coexistence; and – most interestingly – (iii) correlated coexistence. These findings are contrasted with predictions from the mean-field phase diagram and are confirmed by extensive computer simulations of the microscopic dynamics.

PACS. 87.23.Cc Population dynamics and ecological pattern formation – 87.23.Ge Dynamics of social systems

1 Introduction

In biological systems, the survival of a species depends on the frequencies of its kin and its foes in the environment [3,29]. In some cases, the chance of survival of a certain species *improves* as the frequency of its kind increases, since this might enhance the chance for reproduction or other benefits from group interaction. This is denoted as *positive* frequency dependence. In other cases a *negative* frequency dependence, that is the increase of the survival chance with *decreasing* frequency, is observed. This is the case, when individuals compete for rare ressources. Moreover, negative frequency dependence is known to be important for maintaining the genetic diversity in natural populations [24,38].

Frequency dependent dynamics are not only found in biological systems, but also in social and economic systems [2,8,21,26,34,39,42,52]. In democracies, a simple example is a public vote, where the winning chances of a party increase with the number of supporters [7,12]. In economics, e.g. the acceptance of a new products may increase with the number of its users [35]. In stock markets, on the other hand, positive and negative frequency dependencies may interfere. For instance, the desire to buy a certain stock may increase with the orders observed from others, a phenomenon known as the *herding effect*, but it also may decrease, because traders fear speculative bubbles.

In general, many biological and socio-economic processes are governed by the frequency dependent adoption of a certain behavior or strategy, or simply by frequency dependent reproduction. In order to model such dynamics more rigorously (but less concrete), different versions of *voter models* have been investigated. The voter model denotes a simple binary system comprised of N *voters*, each of which can be in one of two states (where *state* could stand for opinion, attitude, or occupation etc.), $\theta_i = \{0, 1\}$. Here, the transition rate $w(\theta|\theta')$ from state θ' to state θ is assumed to be proportional to the frequency f_θ. In this paper, we extend this approach by assuming a *nonlinear* voter model, where the frequency dependence of the transition rate, $w(\theta|\theta') = \kappa(f)\, f_\theta$, includes an additional nonlinearity expressed in terms of the (frequency dependent) prefactor κ.

Linear voter models have been discussed for a long time in mathematics [13,20,27,28]. Recently, they gained more attention in statistical physics [5,6,9,10,14,16,26,30,37,44,45,47,48,50] because of some remarkable features in their dynamics described in Section 2.2. But voter models also found the interest of population biologists [18,22,23,29,33,36].

[a] e-mail: fschweitzer@ethz.ch

Dependent on how the frequency f_θ is estimated, one can distinguish global from local voter models. In the latter case the transition is governed only by the local frequency of a certain state in a given neighborhood. In contrast to global (or mean-field) models, this leads to local effects in the dynamics, which are of particular interest in the current paper. If space is represented by a two-dimenional lattice and each site is occupied by just one individual, then each species occupies an amount of space proportional to its presence in the total population. Local effects such as the occupation of a neighborhood by a particular species or the adoption of a given opinion in a certain surrounding, can then be observed graphically in terms of domain formation. This way, the invasion of species (or opinions) in the environment displays obvious analogies to spatial pattern formation in physical systems.

Physicists have developed different spatial models for such processes. One recent example is the so-called "Sznajd model" [4,7,43] which is a simple cellular automata (CA) approach to consensus formation (i.e. complete invasion) among two opposite opinions (described by spin up or down). In [4], we have shown that the Sznajd model can be completely reformulated in terms of a linear voter model, where the transition rates towards a given opinion are directly proportional to the frequency of the respective opinion of the *second-nearest* neighbors and independent of the nearest neighbors.

Other spatial models are proposed for game-theoretical interactions among nearest neighbors [32,49]. Here, the dynamics are driven by local payoff differences of adjacent players, which basically determine the nonlinearity $\kappa(f)$. Dependent on these payoff differences, we could derive a phase diagram with five regimes, each characterized by a distinct spatio-temporal dynamic [41]. The corresponding spatial patterns range from complete invasion to coexistence with large domains, coexistence with small clusters, and spatial chaos.

In this paper, we are interested in the local effects of frequency dependent dynamics in a homogeneous network, where each site has $m = 4$ nearest neighbors. In this case, the nonlinearity $\kappa(f)$ can be simply expressed by two constants, α_1, α_2. This is a special form of a nonlinear voter model, which for $\alpha_1 < \alpha_2 < 0.5$ also includes majority voting and for $\alpha_1 > \alpha_2 > 0.5$ minority voting. We investigate the dynamics of this model both analytically and by means of computer simulations on a two-dimensional stochastic CA (which is a special form of a homogeneous network with $m = 4$). The latter one was already studied in [29], in particular there was a phase diagram obtained via numerical simulations. In our paper, we go beyond that approach by deriving the phase diagram from an analytical approximation, which is then compared with our own simulations.

In Sections 2, 3.1 we introduce the microscopic model of frequency dependent invasion and demonstrate in Sections 4.1, 4.5 the role of α_1, α_2 by means of characteristic pattern formation. Based on the microscopic description, in Section 3.2 we derive the dynamics for the global frequency $x(t)$, which is a macroscopic key variable. An analytical investigation of these dynamics is made possible by pair approximation, Section 3.3, which results in a closed-form description for $x(t)$ and the spatial correlations $c_{1|1}(t)$. In Section 5.1, we verify the performance of our analytical approximations by comparing them with averaged CA computer simulations. The outcome of the comparison allows us to derive in Section 5.2 a phase diagram in the (α_1, α_2) parameter space, to distinguish between two possible dynamic scenarious: (i) complete invasion of one of the species, with formation of domains at intermediate time scales; and (ii) random spatial coexistence of two species. A third dynamic regime, the nonstationary coexistence of the two species on long time scales together with the formation of spatial domains, can be found in a small, but extended region that separates the two dynamic regimes mentioned above. We further discuss in Section 6 that the usual distinctions for the dynamics, such as positive or negative frequency dependence, do not necessarily coincide with the different dynamic regimes. Instead, for positive frequency dependence, all of the three different dynamic regimes (and the related spatio-temporal patterns) are observed. In the Appendix, calculation details for the pair approximation are given.

2 Formal approach to voter models

2.1 Defining the system

We consider a model of two species labeled by the index $\sigma = \{0, 1\}$. The total number of individuals is constant, so the global frequency x_σ (or the share of each species in the total population) is defined as:

$$N = \sum_\sigma N_\sigma = N_0 + N_1 = \text{const.}$$
$$x_\sigma = \frac{N_\sigma}{N}; \quad x \equiv x_1 = 1 - x_0. \tag{1}$$

In the following, the variable x shall refer to the global frequency of species 1.

The individuals of the two species are identified by the index $i \in N$ and can be seen as nodes of a network. A discrete value $\theta_i \in \{0, 1\}$ indicates whether the node is occupied by species 0 or 1. The network topology (specified later) then defines the nearest neighbors i_j of node i. In this paper, we assume homogeneous networks where all nodes have the same number m of nearest neighbors. For further use, we define the local occupation $\underline{\theta}_i$ of the nearest neighborhood (without node i) as:

$$\underline{\theta}_i = \{\theta_{i_1}, \theta_{i_2}, ..., \theta_{i_m}\}. \tag{2}$$

A specific realization of this distribution shall be denoted as $\underline{\sigma}$, while the function $\underline{\eta}_i(\underline{\sigma})$ assigns $\underline{\sigma}$ to a particular neighborhood $\underline{\theta}_i$:

$$\underline{\sigma} = \{\sigma_1, \sigma_2, ..., \sigma_m\}$$
$$\underline{\eta}_i(\underline{\sigma}) = \{\theta_{i_1} = \sigma_1, \theta_{i_2} = \sigma_2, ..., \theta_{i_m} = \sigma_m\}. \tag{3}$$

For later use, it is convenient to define these distributions also for the nearest neighborhood *including* node i:

$$\underline{\theta}_i^0 = \{\theta_i, \theta_{i_1}, \theta_{i_2}, ..., \theta_{i_m}\} = \underline{\theta}_i \cup \{\theta_i\}$$

$$\underline{\sigma}^0 = \{\sigma, \sigma_1, \sigma_2, ..., \sigma_m\}$$

$$\underline{\eta}_i^0(\underline{\sigma}^0) = \{\theta_i = \sigma, \theta_{i_1} = \sigma_1, \theta_{i_2} = \sigma_2, ..., \theta_{i_m} = \sigma_m\}. \quad (4)$$

For $m = 4$, $\underline{\sigma}^0$ denotes a binary string, e.g. $\{01001\}$, where the first value σ refers to the center node and the other values $\sigma_j \in \{0, 1\}$ indicate the particular values of the nearest neighbors. The assignment of these values to a particular neighborhood $\underline{\theta}_i^0$ of node i is then described by $\underline{\eta}_i^0(\underline{\sigma}^0)$.

In the voter model described in the following section, the dynamics of θ_i is governed by the *occupation distribution* of the *local neighborhood*. that surrounds each node i. Using a stochastic approach, the probability $p_i(\theta_i, t)$ to find node i in state θ_i therefore depends in general on the local occupation distribution $\underline{\theta}_i$ of the neigborhood (Eq. (2)), in the following manner:

$$p_i(\theta_i, t) = \sum_{\underline{\theta}_i'} p(\theta_i, \underline{\theta}_i', t). \quad (5)$$

Hence, $p_i(\theta_i, t)$ is defined as the marginal distribution of $p(\theta_i, \underline{\theta}_i, t)$, where $\underline{\theta}_i'$ in equation (5) indicates the summation over all possible realizations of the local occupation distribution $\underline{\theta}_i$, namely 2^m different possibilities.

For the time dependent change of $p_i(\theta_i, t)$ we assume the following master equation:

$$\frac{d}{dt} p_i(\theta_i, t) = \sum_{\underline{\theta}_i'} \Big[w(\theta_i | (1-\theta_i), \underline{\theta}_i')\; p(1-\theta_i, \underline{\theta}_i', t) - w(1-\theta_i | \theta_i, \underline{\theta}_i')\; p(\theta_i, \underline{\theta}_i', t) \Big] \quad (6)$$

where $w(\theta_i|(1-\theta_i), \underline{\theta}_i)$ denotes the transition rate for state $(1-\theta_i)$ of node i into state θ_i in the next time step under the condition that the local occupation distribution is given by $\underline{\theta}_i$. The transition rate for the reverse process is $w(1-\theta_i|\theta_i, \underline{\theta}_i)$. Again, the summation is over all possible realizations of $\underline{\theta}_i$, denoted by $\underline{\theta}_i'$. It remains to specify the transition rates, which is done in the following section.

2.2 Linear and nonlinear voter models

Our dynamic assumptions for the change of an individual state θ_i are taken from the so-called voter model (see also Sect. 1), abbreviated as VM in the following. The dynamics is given by the following update rule: a voter, i.e. a node $i \in N$ of the network, is selected at random and adopts the state of a randomly chosen nearest neighbor j. After N such update events, time is increased by 1.

The probability to choose a voter with a given state σ from the neighborhood i_j of voter i is directly proportional to the relative number (or frequency) of voters with that particular state in that neigborhood. Let us define the *local frequencies* in the neighborhood as:

$$f_i^\sigma = \frac{1}{m} \sum_{j=1}^{m} \delta_{\sigma\theta_{i_j}}; \quad f_i^{(1-\sigma)} = 1 - f_i^\sigma \quad (7)$$

where δ_{xy} is the Kronecker delta, which is 1 only for $x = y$ and zero otherwise. Then the transition rate of voter i to change its state θ_i does not explicitly depend on the local distribution $\underline{\theta}_i$, but only on the *occupation frequency* f_i^σ, i.e. on the number of nodes occupied by either 0 or 1 in the neighborhood of size m. Hence, the VM describes a frequency dependent dynamics: the larger the frequency of a given state in the neighborhood, the larger the probability of a voter to switch to that particular state *if* it is not already in that state. I.e. the transition rate $w(1-\theta_i|\theta_i = \sigma, f_i^\sigma)$, to *change* state θ increases only with the local frequency of *opposite* states, $f_i^{1-\sigma}$, in the neighborhood:

$$w(1-\theta_i|\theta_i = \sigma, f_i^\sigma) = \gamma f_i^{1-\sigma}. \quad (8)$$

The prefactor γ determines the time scale of the transitions and is set to $\gamma = 1$. Equation (8), describes the dynamics of the *linear* VM because, according to the above update rule, the rate to *change* the state is directly proportional to the frequency.

The linear (or standard) VM has two remarkable features. First, it is known that, starting from a random distribution of states, the system always reaches a completely ordered state, which is often referred to as *consensus* in a social context, or complete *invasion* in a population biology context. As there are individuals with two different states, the complete ordered state can be either all 0 or all 1. Which of these two possible attractors of the dynamics is eventually reached, depends (in addition to stochastic fluctuations) on the initial global frequency, i.e. $x(t = 0)$. It has been shown that, for an ensemble average, the frequency of the outcome of a particular consensus state 1 is equal to the initial frequency $x(t = 0)$ of state 1. This second remarkable feature is often denoted as conservation of magnetization, where the magnetization is defined as $M(t) = x_1(t) - x_0(t) = 2x(t) - 1$. Hence, consensus means $|M| = 1$. Thus we have the interesting situation that, for a single realization, the dynamics of the linear VM is a fluctuation driven process that, for finite system sizes, always reaches consensus, whereas on average the outcome of the consensus state is distributed as $x(0)$.

The (only) interesting question for the linear VM is then how long it may take the system to reach the consensus state, dependent on the system size N and the network topology. The time to to reach consensus, T_κ, is obtained through an average over many realizations. As the investigation of T_κ is not the focus of our paper (see [19,25,48]), we just mention some known results for the linear VM: one finds for one-dimensional regular lattices $(d = 1)$ $T_\kappa \propto N^2$ and for two-dimensional regular lattices $(d = 2)$ $T_\kappa \propto N \log N$. For $d > 2$ the system does not always reach an ordered state in the thermodynamic limit. In finite systems, however, one finds $T_\kappa \sim N$.

While the linear VM has some nice theoretical properties, it also has several conceptual disadvantages when applying the model to a social or population biological context. First of all, the "voters" do not vote in this model, they are subject to a random (but frequency based) assignment of an "opinion", without any choice. Secondly, the state of the voter under consideration does not play any role in the dynamics. This can be interpreted in a social context as a (blind) herding dynamics, where the individuals just adopt the opinion of the majority. In a population model of two competing species, it means that individuals from a minority species may be replaced by those from a majority species without any resistance.

In order to give voter i at least some weight compared to the influence of its neighbors i_j, one can simply count its state θ_i into the local frequency f_i^σ, i.e. instead of equations (2), (3) we may use equation (4). Using for voter i the notation $\theta_i \equiv \theta_{i_0}$ (i.e. $j=0$), we can still use equation (8) for the transition rates, with the noticeable difference that the local frequency f_i^σ of equation (7) is now calculated from a summation that starts with $j = 0$. The explicit consideration of θ_i thus has the effect of adding some *inertia* to the dynamics. In fact, extending the summation to $j = 0$ multiplies the transition rate, equation (8), by a factor $m/(m+1)$, where m is the number of nearest neighbors. I.e., for $m = 4$ a local configuration $\underline{\sigma}^0 = \{01001\}$ would lead to a transition rate $w(1|0) = 0.5$ *without* the additional inertia, but $w(1|0) = 0.4$ by counting in the state of voter i. I.e., taking into account the state of voter i considerably reduces the transition rate towards the opposite state.

We find it useful for conceptual reasons to include some resistance into the model and therefore will use from now on the description which takes the current state of voter i into account. This also has the nice advantage that for the case $m = 4$, which describes e.g. square lattices, we avoid stalemate situations, $w(1 - \theta|\theta) = 0.5$. However, we note that the addition of the constant resistance does not change the dynamics of the model, as it only adjusts the *time scale* towards a new factor $\gamma' = (m/m + 1)\,\gamma$. So, keeping m constant and equal for all voters, we can rescale $\gamma' = 1$.

We note that there are of course other ways to give some weight to the opinion of voter i. In [45,46], we have discussed a modified VM, where voters additionally have an inertia $\nu_i \in [0, 1]$ which leads to a decrease of the transition rate to change their state:

$$w^R(1 - \theta_i|\theta_i) = (1 - \nu_i)\; w(1 - \theta_i|\theta_i) \tag{9}$$

here $w(1-\theta|\theta)$ is given by the linear VM, equation (8). The individual inertia ν_i is evolving over time by assuming that it increases with the persistence time τ_i the voter has been keeping its current state. While this inertia may slow down the microscopic dynamics of the VM and thus may increase the time to reach consensus, T_κ, we found the counterintuitive result that under certain circumstances a decelerated microdynamics may even accelerate the macrodynamics of the VM, thus decreasing T_κ compared to the linear VM.

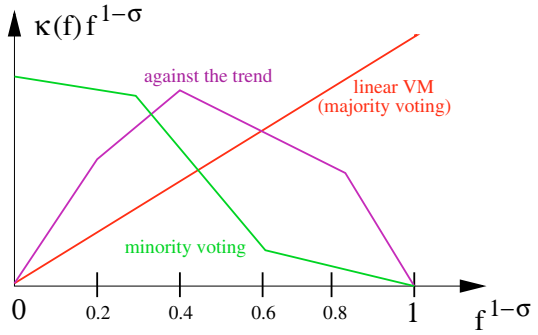

Fig. 1. Different nonlinear frequency dependencies for equation (10). Note the piecewise linear functions, as the number of neighbors m and thus the frequencies f have mostly discrete values.

The addition of a nonlinear inertia to the VM, equation (9), is a special case for turning the linear VM into a nonlinear one (whereas the fixed resistance would not change the linear VM). In general, nonlinear VM can be expressed as

$$w(1-\theta_i|\theta_i=\sigma, f_i^\sigma) = \kappa(f)\; f_i^{1-\sigma} \tag{10}$$

where $\kappa(f)$ is a nonlinear, frequency dependent function describing how voter i reacts on the occurrence of opposite "opinions" in its immediate neighborhood. Figure 1 shows some possible examples which have their specific meaning in a social context. Whereas any function $\kappa(f) = \text{const.} > 0$ describes the linear VM, i.e. a majority voting or herding effect, a decreasing $\kappa(f)$ means minority voting, i.e. the voter tends to adopt the opinion of the minority. Nonmonotonous $\kappa(f)$ can account for voting against the trend, i.e. the voter adopts an opinion as long as this is not already the ruling opinion – a phenomenon which is important e.g. in modeling the adoption of fashion. An interpretation of these functions in a population biology context will be given in Section 4.1

In conclusion, introducing the nonlinear response function $\kappa(f)$ will allow us to change the global dynamics of the linear VM. Instead of reaching always consensus, i.e. the exclusive domination of one "opinion" or species, we may be able to observe some more interesting macroscopic dynamics, for example the coexistence of both states. It is one of the aims of this paper to find out, under which specifications of $\kappa(f)$ we may in fact obtain a dynamic transition that leads to a a structured, but not fully ordered state instead of a completely ordered state.

3 Stochastic dynamics of the voter model

3.1 Microscopic dynamics

In order to give a complete picture of the dynamics of the nonlinear VM, we have to derive the stochastic dynamics for the *whole* system of N nodes, whereas equation (6) gives us "only" the *local* dynamics in the vicinity of a

particular voter i. For N voters, the distribution of states is given by

$$\Theta = \{\theta_1, \theta_2, ..., \theta_N\}. \tag{11}$$

Note that the state space Ω of all possible configurations is of the order 2^N. In a stochastic model, we consider the probability $p(\Theta, t)$ of finding a particular configuration at time t. If t is measured in discrete time steps (generations) and the network is synchronously updated, the time-dependent change of $p(\Theta, t)$ is described as follows:

$$p(\Theta, t + \Delta t) = \sum_{\Theta'} p(\Theta, t + \Delta t | \Theta', t) p(\Theta', t) \tag{12}$$

where Θ' denotes all possible realizations of Θ and $p(\Theta, t+\Delta t|\Theta', t)$ denote the conditional probabilities to go from state Θ' at time t to Θ at time $t + \Delta t$. Equation (12) is based on the Markov assumption that the dynamics at time $t + \Delta t$ may depend only on states at time t. With the assumption of small time steps Δt and the definition of the transition rates

$$w(\Theta|\Theta', t) = \lim_{\Delta t \to 0} \frac{p(\Theta, t + \Delta t|\Theta', t)}{\Delta t} \tag{13}$$

equation (12) can be transferred into a time-continuous master equation as follows:

$$\frac{d}{dt} p(\Theta, t) = \sum_{\Theta'} \Big[w(\Theta|\Theta')\, p(\Theta', t) - w(\Theta'|\Theta)\, p(\Theta, t) \Big]. \tag{14}$$

In equation (14), the transition rates depend on the *whole* distribution Θ. However, in the frequency dependent dynamics introduced in Section 2.1, only the occupation distribution of the *local* neighborhood of node i needs to be taken into account. Therefore, it is appropriate to think about some reduced description in terms of lower order distributions, such as the local occupation $\underline{\theta}_i$, equation (2). In principle, there are two different ways to solve this task. The first one, the *top-down* approach starts from the *global* distribution Θ in the whole state space and then uses different approaches to factorize $p(\Theta, t)$. However, a Markov analysis [31] can only be carried out exactly for small N, because of the exponential N-dependence of the state space. Thus, for larger N suitable approximations, partly derived from theoretical concepts in computer science need to be taken into account.

In this paper, we follow a second way which is a *bottom-up* approach based on the *local* description already given in Section 2.1. I.e. starting from node i and its local neighborhood, we want to derive the dynamics for some appropriate *macroscopic* variables describing the nonlinear VM. Instead of one equation for $p(\Theta, t)$ in the top-down approach, in the bottom-up approach we now have a set of N stochastic equations for $p_i(\theta_i, t)$, equation (14), which are locally coupled because of overlapping neighborhoods, $\underline{\theta}_i$. In order to solve the dynamics, we need to discuss suitable approximations for these local correlations. As we are interested in the macroscopic dynamics, these approximations will be done at the macroscopic level. In order to do so, we first derive a macroscopic equation from the stochastic equation (6), which is carried out in the following section.

3.2 Derivation of the macroscopic dynamics

The key variable of the macroscopic dynamics is the global frequency $x_\sigma(t)$, defined in equation (1). In order to compare the averaged computer simulations with results from analytical approximations later in Section 5, we first derive an equation for the expectation value $\langle x_\sigma \rangle$. We do this without an explicit determination of the transition rates and wish to emphasize that the formal approach presented in Section 3 remains valid not just for the voter model, but also for other dynamic processes which depend on neighbor interactions (not only nearest neighbors) in various network topologies.

For the derivation of the expectation value we start from the stochastic description given in Section 3.1, where $p(\Theta, t)$ denoted the probability to find a particular distribution Θ, equation (11), at time t and Θ' denoted all possible realizations of Θ equation (14). On one hand:

$$\begin{aligned} \langle x_\sigma(t) \rangle &= \frac{1}{N} \sum_{\Theta'} \left(\sum_{i=1}^{N} \delta_{\sigma\theta_i} \right) p(\Theta', t) \\ &= \frac{1}{N} \sum_{\Theta'} N_\sigma\, p(\Theta', t) = \frac{\langle N_\sigma(t) \rangle}{N} \end{aligned} \tag{15}$$

and on the other hand:

$$\begin{aligned} \langle x_\sigma(t) \rangle &= \frac{1}{N} \sum_{i=1}^{N} \sum_{\Theta'} \delta_{\sigma\theta_i}\, p(\Theta', t) \\ &= \frac{1}{N} \sum_{i=1}^{N} p_i(\theta_i = \sigma, t). \end{aligned} \tag{16}$$

By differentiating equation (16) with respect to time and inserting the master equation (6), we find the following macroscopic dynamics for the network:

$$\begin{aligned} \frac{d}{dt} \langle x_\sigma(t) \rangle = \frac{1}{N} \sum_{i=1}^{N} \sum_{\underline{\theta}'_i} \Big[& w(\sigma|(1-\sigma), \underline{\theta}'_i) \\ & \times p(\theta_i = (1-\sigma), \underline{\theta}'_i, t) \\ & - w(1-\sigma|\sigma, \underline{\theta}'_i)\, p(\theta_i = \sigma, \underline{\theta}'_i, t) \Big]. \end{aligned} \tag{17}$$

For the further treatment of equation (17), we consider a specific distribution of states on $m+1$ nodes defined by $\underline{\sigma}^0$. This distribution is assigned to a particular neighborhood of node i by $\underline{\eta}_i^0(\underline{\sigma}^0)$ (Eq. (4)). Since we are interested in how many times a special realization of a specific distribution $\underline{\sigma}^0$ is present in the population, we define an indicator function

$$\chi(\underline{\eta}_i^0) \equiv \chi_{\underline{\sigma}^0}(\underline{\eta}_i^0(\underline{\sigma}^0)) = \delta_{\underline{\theta}_i \underline{\sigma}^0} \tag{18}$$

that is 1 if the neighborhood of node i has the distribution $\underline{\sigma}^0$, and 0 otherwise. Therefore, we write the frequency of the n-tuplet $\underline{\sigma}^0$ in the population as:

$$x_{\underline{\sigma}^0}(\Theta) := \frac{1}{N} \sum_{i=1}^{N} \chi(\underline{\eta}_i^0). \tag{19}$$

The expectation value is

$$\langle x_{\underline{\sigma}^0}(t)\rangle = \sum_{\Theta'} x_{\underline{\sigma}^0}(\Theta')\; p(\Theta', t). \tag{20}$$

Inserting equation (19) into equation (20), we verify that

$$\begin{aligned}\langle x_{\underline{\sigma}^0}(t)\rangle &= \frac{1}{N}\sum_{i=1}^{N}\sum_{\Theta'} \chi(\underline{\eta}_i^0)\; p(\Theta', t)\\ &= \frac{1}{N}\sum_{i=1}^{N} p(\underline{\eta}_i^0, t)\end{aligned} \tag{21}$$

because of the definition of the marginal distribution. Using the identity $p(\underline{\eta}_i^0, t) = p(\sigma, \underline{\eta}_i, t)$, we may rewrite equation (17) by means of equation (21) to derive the macroscopic dynamics in the final form:

$$\begin{aligned}\frac{d}{dt}\langle x_\sigma(t)\rangle = \sum_{\underline{\sigma}'} \Big[& w(\sigma|(1-\sigma), \underline{\sigma}')\; \langle x_{(1-\sigma),\underline{\sigma}'}(t)\rangle \\ & - w(1-\sigma|\sigma, \underline{\sigma}')\; \langle x_{\sigma,\underline{\sigma}'}(t)\rangle \Big]\end{aligned} \tag{22}$$

$\underline{\sigma}'$ denotes the 2^m possible configurations of a specific occupation distribution $\underline{\sigma}$, equation (3). In the following, we use $\langle x\rangle \equiv \langle x_1\rangle = 1 - \langle x_0\rangle$. Then, the dynamic for $\langle x\rangle$ reads:

$$\begin{aligned}\frac{d}{dt}\langle x(t)\rangle = \sum_{\underline{\sigma}'} \Big[& w(1|0, \underline{\sigma}')\; \langle x_{0,\underline{\sigma}'}(t)\rangle \\ & - w(0|1, \underline{\sigma}')\; \langle x_{1,\underline{\sigma}'}(t)\rangle \Big].\end{aligned} \tag{23}$$

The solution of equation (23) would require the computation of the averaged global frequencies $\langle x_{1,\underline{\sigma}}\rangle$ and $\langle x_{0,\underline{\sigma}}\rangle$ for all possible occupation patterns $\underline{\sigma}$, which would be a tremendous effort. Therefore, in the next section we will introduce two analytical approximations to solve this problem. In Section 5.1 we will further show by means of computer simulations that these approximations are able to describe the averaged dynamics of the nonlinear VM.

3.3 Mean-field limit and pair approximation

As a first approximation of equation (23), we investigate the mean-field limit. Here the state of each node does not depend on the occupation distribution of its neighbors, but on m randomly chosen nodes. In this case the occupation distribution factorizes:

$$\langle x_{\underline{\sigma}^0}\rangle = \langle x_\sigma\rangle \prod_{j=1}^{m} \langle x_{\sigma_j}\rangle. \tag{24}$$

For the macroscopic dynamics, equation (23), we find:

$$\begin{aligned}\frac{d}{dt}\langle x(t)\rangle = \sum_{\underline{\sigma}'} \Big[& w(1|0, \underline{\sigma}')\,(1 - \langle x\rangle) \prod_{j=1}^{m} \langle x_{\sigma_j}\rangle \\ & - w(0|1, \underline{\sigma}')\; \langle x\rangle \prod_{j=1}^{m} \langle x_{\sigma_j}\rangle \Big].\end{aligned} \tag{25}$$

For the calculation of the $\langle x\rangle_{\sigma_j}$ we have to look at each possible occupation pattern $\underline{\sigma}$ for a neighborhood m. This will be done in detail in Section 4.1. Before, we discuss another analytical approximation which solves the macroscopic equation (23) with respect to *correlations*. This is the so-called *pair approximation*, where one is not interested in the occupation distribution of a whole neighborhood $\underline{\sigma}^0$, equation (4) but only in *pairs* of nearest neighbor nodes, σ, σ' with $\sigma' \in \{0, 1\}$. That means the local neighborhood of nearest neighbors is decomposed into pairs, i.e. blocks of size 2 that are called *doublets*.

Similar to equation (19), the global frequency of doublets is defined as:

$$x_{\sigma,\sigma'} = \frac{1}{N}\sum_{i=1}^{N}\sum_{j=1}^{m}\frac{1}{m}\;\chi(\theta_i = \sigma, \theta_{i_j} = \sigma'). \tag{26}$$

The expected value of the doublet frequency is then given by $\langle x_{\sigma,\sigma'}\rangle$ in the same way as in equation (20). We now define the correlation term as:

$$c_{\sigma|\sigma'} := \frac{\langle x_{\sigma,\sigma'}\rangle}{\langle x_{\sigma'}\rangle} \tag{27}$$

neglecting higher order correlations. Thus $c_{\sigma|\sigma'}$ can be seen as an approximation of the conditional probability that a randomly chosen nearest neighbor of a node in state σ' is in state σ. Using the above definitions, we have the following relations:

$$\langle x_{\sigma'}\rangle\, c_{\sigma|\sigma'} = \langle x_\sigma\rangle\, c_{\sigma'|\sigma}; \quad \sum_{\sigma'\in\{0,1\}} c_{\sigma'|\sigma} = 1. \tag{28}$$

For the case of two species $\sigma \in \{0, 1\}$, $c_{1|1}$ and $c_{0|0}$ are the *inter-species* correlations, while $c_{1|0}$ and $c_{0|1}$ denote the *intra-species* correlations. Using $\langle x\rangle \equiv \langle x_1\rangle$, these correlations can be expressed in terms of only $c_{1|1}$ and $\langle x\rangle$ as follows:

$$\begin{aligned} c_{0|1} &= 1 - c_{1|1}\\ c_{1|0} &= \frac{\langle x\rangle\;(1 - c_{1|1})}{1 - \langle x\rangle}\\ c_{0|0} &= \frac{1 - 2\,\langle x\rangle + \langle x\rangle\, c_{1|1}}{1 - \langle x\rangle}.\end{aligned} \tag{29}$$

Now, the objective is to express the global frequency of a specific occupation pattern $\langle x_{\underline{\sigma}^0}\rangle$, equation (20), in terms of the correlation terms $c_{\sigma|\sigma'}$. In pair approximation, it is assumed that the states θ_{i_j} are correlated only through the state θ_i and uncorrelated otherwise. Then the global frequency terms in equation (22) can be approximated as follows:

$$\langle x_{\underline{\sigma}^0}\rangle = \langle x_\sigma\rangle \prod_{j=1}^{m} c_{\sigma_j|\sigma}. \tag{30}$$

For the macroscopic dynamics, equation (23), we find in pair approximation:

$$\begin{aligned}\frac{d}{dt}\langle x(t)\rangle = \sum_{\underline{\sigma}'} \Big[& w(1|0, \underline{\sigma}')\,(1 - \langle x\rangle) \prod_{j=1}^{m} c_{\sigma_j|\sigma} \\ & - w(0|1, \underline{\sigma}')\; \langle x\rangle \prod_{j=1}^{m} c_{\sigma_j|(1-\sigma)} \Big].\end{aligned} \tag{31}$$

Note that the $c_{\sigma_j|\sigma}$ can be expressed in terms of $c_{1|1}$ by means of equation (29). Thus, equation (31) now depends on only two variables, $\langle x\rangle$ and $c_{1|1}$. In order to derive a *closed* form description, we need an additional equation for $\dot{c}_{1|1}$. That can be obtained from equation (27):

$$\frac{dc_{1|1}}{dt} = -\frac{c_{1|1}}{\langle x\rangle}\frac{d}{dt}\langle x\rangle + \frac{1}{\langle x\rangle}\frac{d}{dt}\langle x_{1,1}\rangle\,. \tag{32}$$

Equation (32) also requires the time derivative of the global doublet frequency $\langle x_{1,1}\rangle$. Even in their lengthy form, the three equations for $\langle x\rangle$, $c_{1|1}$, $\langle x_{1,1}\rangle$ can easily be solved numerically. This gives the approach some computational advantage compared to averaging over a number of microscopic computer simulations for all possible parameter sets.

Although the approach derived so far is quite general in that it can be applied to different network topologies and neighborhood sizes, specific expressions for these three equations of course depend on these. Therefore, in the Appendix, these three equations are explicitly derived for a $2d$ regular lattice with neighborhood $m = 4$ using the specific transition rates introduced in the next section. In Section 5.1, we further show that the pair approximation yields some characteristic quantities such as $\langle x(t)\rangle$ for the $2d$ regular lattice in very good agreement with the results of computer simulations.

4 Invasion versus coexistence

4.1 Nonlinear response functions

So far, we have developed a stochastic framework for (but not restricted to) nonlinear voter models in a general way, without specifying two of the most important features, namely (i) the network topology which defines the neighborhood, and (ii) the nonlinearity $\kappa(f)$ which defines the response to the local frequencies of the two different states. For (i), let us choose a regular network with $m = 4$, i.e. each voter has 4 different neighbors. We note explicitly that our modeling framework and the general results derived hold for *all homogeneous networks*, but for the visualization of the results it will be most convenient to choose a regular square lattice, where the neighbors appear next to a node. This allows us to observe the formation of macroscopic ordered states in a more convenient way, without restricting the general case. Eventually, to illustrate the dynamics let us now assume a population biology context, where each node is occupied by an individual of either species 0 or 1. The spreading of one particular state is then interpreted as the invasion of that respective species and the local disappearance of the other one, while the emergence of a complete ordered state is seen as the complete invasion or domination of one species together with the extinction of the other one.

Keeping in mind that we also consider the state of node i itself, we can write the possible transition rates, equation (10), for the neighborhood of $n = m+1 = 5$ and $\theta_i = \sigma$ in the following explicit way (cf. also [29]):

f_i^{σ}	$f_i^{(1-\sigma)}$	$w(1-\theta_i\|\theta_i=\sigma, f_i^{\sigma})$
1	0	α_0
4/5	1/5	α_1
3/5	2/5	α_2
2/5	3/5	$\alpha_3 = 1-\alpha_2$
1/5	4/5	$\alpha_4 = 1-\alpha_1$
0	5/5	$\alpha_5 = 1-\alpha_0$

(33)

Equation (33) means that a particular node i currently in state $\theta_i = \sigma$, or occupied by an individual of species σ where σ is either 0 or 1, will be occupied by an individual of species $(1-\sigma)$ with a rate $w(1-\theta_i|\theta_i=\sigma, f_i^{\sigma})$ that changes with the local frequency f_i^{σ} in a *nonlinear* manner. The different values of α_n denote the products $\kappa(f)f_i^{1-\sigma}$ for the specific values of f given. I.e., the α_n define the piecewise linear functions shown in Figure 1.

The general case of six independent transition rates α_n ($n = 0, ..., 5$) in equation (33) can be reduced to three transition rates α_0, α_1, α_2 by assuming a symmetry of the invasion dynamics of the two species, i.e. $\alpha_2+\alpha_3 = 1$, $\alpha_1+\alpha_4 = 1$ and $\alpha_0+\alpha_5 = 1$. Further, assuming a pure frequency dependent process, we have to consequently choose $\alpha_0 = 0$, because in a complete homogeneous neighborhood, there is no incentive to change to another state (there are no other species around to invade).

We recall that if the transition rates α_1, α_2 are directly proportional to $f^{(1-\sigma)}$, i.e. $\alpha_1 = 0.2$ and $\alpha_2 = 0.4$, this recovers the linear VM, equation (8). (Note that without the resistance of node i discussed in Section 2.2 the linear voter point would read as $\alpha_1 = 0.25$ and $\alpha_2 = 0.5$ instead.) Dependent on the relation of the two essential parameters α_1, α_2, we also find different versions of *nonlinear* VM, which have their specific meaning in a population biology context:

$$\begin{aligned}
&\text{(pf)} && 0 \le \alpha_1 \le \alpha_2 \le (1-\alpha_2) \le (1-\alpha_1) \le 1\\
&\text{(nf)} && 1 \ge \alpha_1 \ge \alpha_2 \ge (1-\alpha_2) \ge (1-\alpha_1) \ge 0\\
&\text{(pa)} && 0 \le \alpha_1 \le \alpha_2,\ \alpha_2 \ge (1-\alpha_2),\\
& && (1-\alpha_2) \le (1-\alpha_1) \le 1\\
&\text{(na)} && 1 \ge \alpha_1 \ge \alpha_2,\ \alpha_2 \le (1-\alpha_2),\\
& && (1-\alpha_2) \ge (1-\alpha_1) \ge 0.
\end{aligned} \tag{34}$$

Note, that the parameters $\alpha_1, \ldots, \alpha_4$ can be ordered in 24 different ways. These reduce to 8 inequalities under the conditions $\alpha_3 = 1-\alpha_2$ and $\alpha_4 = 1-\alpha_1$. In equation (34), (pf) means (pure) *positive frequency dependent invasion*, where the transition rate *increases* with an increasing number of individuals of the *opposite* species $(1-\sigma)$ in the neighborhood, and (nf) means (pure) *negative frequency dependent invasion* because the transition rate *decreases*. The two other cases describe positive (pa) and negative (na) *allee effects* [29]. These regions are described by 3 inequalities each, all of which show the same relative change in parameter values, if going from α_1 to α_4. Similar to the drawings in Figure 1 this can be roughly

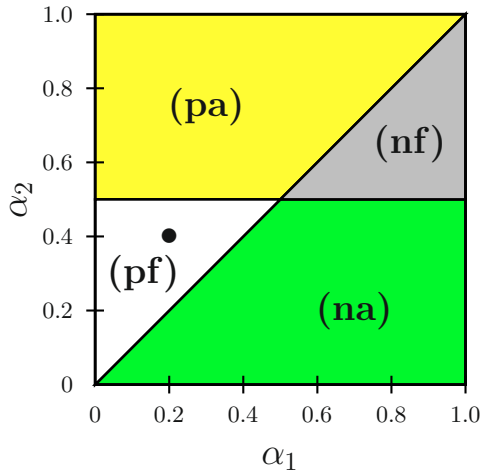

Fig. 2. Four different parameter regions for frequency dependent invasion, according to equation (34). The linear voter point is indicated by •.

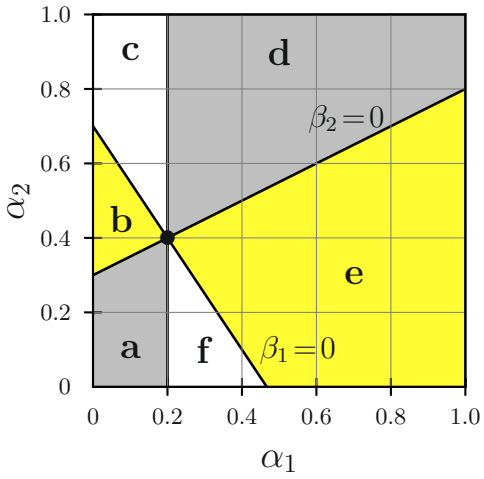

Fig. 3. Phase diagram of the invasion dynamics in the mean-field case. For the different areas see text. The functions $\beta_1 = 0$ and $\beta_2 = 0$ are given by equation (36). The areas in lighter gray indicate imaginary solutions of $x^{(4,5)}$, equation (36) while the areas in darker gray (color: yellow) indicate solutions of $x^{(4,5)}$ outside the $\{0, 1\}$ interval. The linear voter point is indicated by •. Note that the physically relevant solutions $x^{1,2,3}$ are the same in the lighther gray and darker gray (color: yellow) areas, however their stability is different in (a, b) and (d, e).

visualized as an up-down-up change in region (pa) and a down-up-down change in region (na). The different parameter regions are shown in Figure 2. On a first glimpse, one would expect that the dynamics as well as the evolution of global variables may be different in these regions. Thus, one of the aims of this paper is to investigate whether or to what extent this would be the case.

4.2 Mean-field analysis

In order to find out about the influence of the nonlinear response function $\kappa(f)$, which is specified here in terms of α_1, α_2, let us start with the mean-field approach that lead to equation (25). As we outlined in Section 3.3, the calculation of the $\langle x_{\sigma_j} \rangle$ in equation (25) requires to look at each possible occupation pattern $\underline{\sigma}$ for a neighborhood m, for instance, $\underline{\sigma} = \{0010\}$. The mean-field approach assumes that the occurence of each 1 or 0 in the pattern can be described by the global frequencies x and $(1-x)$, respectively (for simplicity, the abbreviation $x \equiv \langle x \rangle$ will be used in the following). For the example of string $\underline{\sigma} = \{0010\}$ we find $\prod \langle x_{\sigma_j} \rangle = x(1-x)^3$. The same result yields for $\underline{\sigma} = \{0100\}$ and for any other string that contains the same number of 1 and 0, i.e. there are exactly $\binom{4}{1}$ different possibilities. For strings with two nodes of each species, $\binom{4}{2}$ times the contribution $\prod \langle x_{\sigma_j} \rangle = x^2(1-x)^2$ results, etc. Inserting Eq. (33) for the transition rates, we find with $\alpha_0 = 0$ the equation for the mean-field dynamics:

$$\begin{aligned}\frac{dx}{dt} = {} & (1-x)\Big[4\alpha_1 x(1-x)^3 + 6\alpha_2 x^2(1-x)^2 \\ & + 4(1-\alpha_2)x^3(1-x) + (1-\alpha_1)x^4\Big] \\ & - x\Big[(1-\alpha_1)(1-x)^4 + 4(1-\alpha_1)x(1-x)^3 \\ & + 6\alpha_2 x^2(1-x)^2 + 4\alpha_1 x^3(1-x)\Big]. \end{aligned} \quad (35)$$

The fixed points of the mean-field dynamics can be calculated from equation (35) using $\dot{x} = 0$. We find:

$$\begin{aligned} x^{(1)} = 0; \quad x^{(2)} = 1; \quad x^{(3)} = 0.5 \\ x^{(4,5)} = 0.5 \pm \sqrt{\beta_1/4\beta_2} \\ \beta_1 \equiv \alpha_2 + 1.5\alpha_1 - 0.7; \; \beta_2 \equiv \alpha_2 - 0.5\alpha_1 - 0.3. \end{aligned} \quad (36)$$

The first three stationary solutions denote either a complete invasion of one species or an equal share of both of them. "Nontrivial" solutions, i.e. a *coexistence* of both species with different shares of the total population, can only result from $x^{(4,5)}$, provided that the solutions are (i) real and (ii) in the interval $\{0, 1\}$. The first requirement means that the two functions β_1, β_2 are either both positive or both negative. The second requirement additionally results in $\alpha_1 \leq 0.2$ if $\alpha_2 \geq 0.4$ and $\alpha_1 \geq 0.2$ if $\alpha_2 \leq 0.4$. This leads to the phase diagram of the mean-field case shown in Figure 3.

In order to verify the stability of the solutions, we have further done a perturbation analysis (see also Sect. 4.4). The results can be summarized as follows:

- in the regions a and b of the mean-field phase diagram, Figure 3, $x^{\text{stat}} = 0$ and $x^{\text{stat}} = 1$ are the only stable fixed points of the dynamics, while $x = 0.5$ is an unstable fixed point (cf. also Fig. 4 top). Species 1 with $x(t=0) < 0.5$ will most likely become extinct, while it will remain as the only survivor for $x(t=0) > 0.5$. Thus, the region (a, b) can be characterized as the region of *invasion*;
- in region c, the mean-field limit predicts the three stable fixed points 0, 1 and 0.5. The attractor basin for

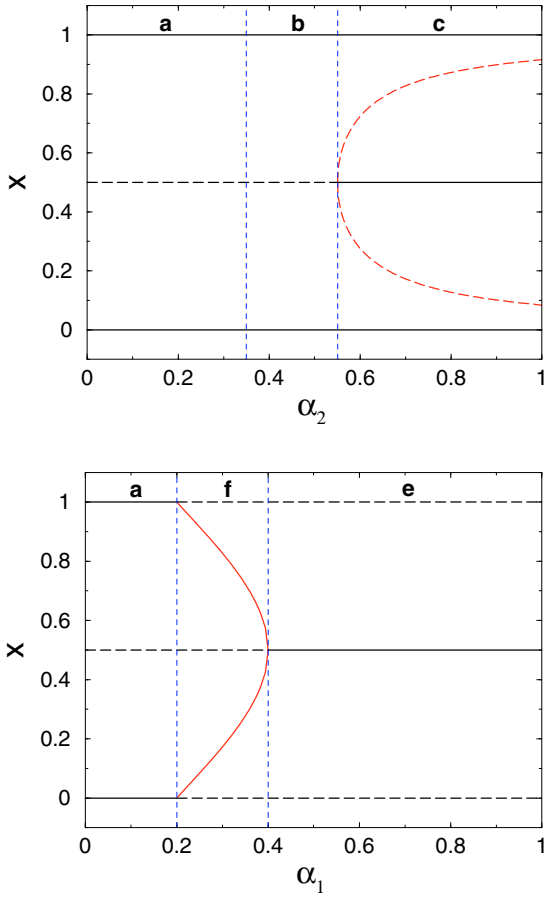

Fig. 4. Bifurcation diagram of the stationary solutions dependent on α_1 and α_2. (top) $\alpha_1 = 0.1$, (bottom) $\alpha_2 = 0.1$. The solid lines refer to stable solutions, the dashed lines to unstable ones. The notations a–f refer to the respective areas in the phase diagram, Figure 3.

0.5 is the largest as Figure 4 (top) indicates. The separatrices are given by the unstable solutions $x^{(4,5)}$, equation (36). In this parameter region, the mean-field limit predicts either *coexistence* of both species with equal shares, or *invasion* of one species, dependent on the initial condition $x(t=0)$;

– in the regions d and e, only one stable fixed point $x^{\rm stat} = 0.5$ can be found, while the solutions 0 and 1 are unstable (cf. also Fig. 4 bottom). Thus, the mean-field approach predicts the *coexistence* of both species with equal share.
– finally, in region f the solutions 0, 1 and 0.5 are unstable fixed points , but the two remaining solutions $x^{(4,5)}$, equation (36) are stable fixed points (cf. Fig. 4 bottom). Thus, this region is the most interesting one, since it seems to enable "nontrivial" solutions, i.e. an *asymmetric coexistence* of both species with different shares. We note again, that this is a prediction of the mean-field analysis. At the intersection of regions f and a, these two solutions approach 0 and 1, while at the intersection of regions f and e they both converge to 0.5.

We will compare these mean-field predictions both with computer simulations and analytical results from the pair approximations later in this paper. Before, in Sections 4.3, 4.4 we would like to point to some interesting (α_1, α_2) combinations in this phase diagram where the mean-field analysis does not give a clear picture of the dynamics.

4.3 Deterministic limit

The first set of interesting points are (α_1, α_2) combinations of values 0 and 1, such as $(\alpha_1, \alpha_2) = (0, 0)$ etc. These cases are special in the sense that they describe the *deterministic* limit of the nonlinear voter dynamics. Whereas for $0 < \alpha_n < 1$ always a finite probability exist to change to the opposite state, for $(0, 0)$ the state of node i *never* changes as long as at least half of the nearest neighbor nodes are occupied by the same species. On the other hand, it will *always* change if more then half of the neighboring nodes are occupied by the *other* species. This refers to a *deterministic* positive frequency invasion process. Similarly, a *deterministic* negative frequency invasion process is described by $(1, 1)$.

The deterministic dynamics, as we know from various other examples, may lead to a completely different outcome as the stochastic counterpart. In order to verify that we have conducted computer simulations using a *cellular automaton* (CA), i.e., a two-dimensional regular lattice with periodic boundary conditions and *synchronous update* of the nodes. The latter one can be argued, but we verified that there are no changes in the results of the computer simulations if the sequential update is used. The time scale for the synchronous update is defined by the number of simulation steps. If not stated otherwise, the initial configuration is taken to be a random distribution (within reasonable limits) of both species, i.e. initially each node is randomly assigned one of the possible states, $\{0, 1\}$. Thus, the initial global frequency is $x(t=0) = 0.5$. Figure 5 shows snapshots of computer simulations of the deterministic dynamics taken in the (quasi-)stationary dynamic regime.

If we compare the snapshots of the *deterministic* voter dynamics with the mean-field prediction, the following observations can be made:

1. a spatial coexistence of both species is observed for the (α_1, α_2) values $(0, 0)$, Figure 5a, $(1, 0)$, Figure 5d, $(1, 1)$, Figure 5b, where the global frequency in the stationary state is $x^{\rm stat} = 0.5$. This contradicts with the mean-field prediction for $(0, 0)$, which is part of region (a) and thus should display complete invasion;
2. a complete invasion of one species is observed for $(\alpha_1, \alpha_2) = (0, 1)$, Figure 5a. This would agree with the mean-field prediction of *either* coexistence *or* invasion. A closer look at the bifurcation diagram, Figure 4 (top), however tells us that for the given intial condition $x(t = 0) = 0.5$ the stationary outcome should be *coexistence*, whereas the deterministic limit shows *always invasion* as was verified by numerous computer simulations with varying initial conditions;

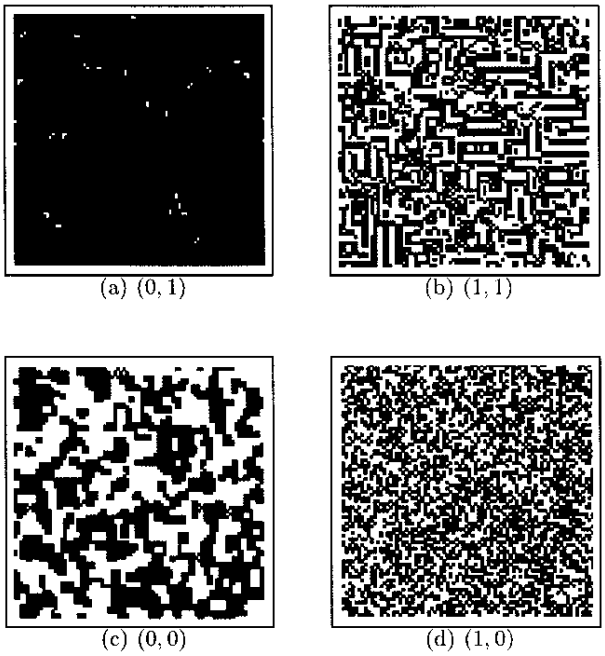

Fig. 5. Spatial snapshots of a deterministic frequency dependent invasion process for different combinations of (α_1, α_2). The pictures are taken after $t = 10^2$ time steps, except for (a), where $t = 10^4$. Lattice size: 80×80. In all pictures black dots refer to species 1.

3. for the deterministic frequency dependent processes $(0, 0)$, $(1, 0)$ the spatial pattern becomes stationary after a short time. For the negative frequency dependence $(1, 1)$ the pattern flips between two different configurations at every time step. So, despite a constant global frequency $x^{\text{stat}} = 0.5$ in the latter case, local reconfigurations prevent the pattern from reaching a completely stationary state, but it may be regarded as (quasi-)stationary, i.e. the macroscopic observables do not change but microscopic changes still occur;
4. in both – positive and negative – deterministic frequency dependence cases, individuals of the same species tend to aggregate in space, albeit in different local patterns. For the positive frequency dependence, we see the occurence of small clusters, Figure 5c, or even complete invasion, Figure 5a, based on the local feedback within the same species. For the negative frequency dependence however we observe the formation of a meander-like structure that is also known from physico-chemical structure formation [40]. It results from the antagonistic effort of each species to avoid individuals of the same kind, when being surrounded by a majority of individuals of the opposite species.

In conclusion, the mean-field analysis given in this section may provide a first indication of how the nonlinearities may influence the voter dynamics. This, however, cannot fully extended to the limiting cases given by the deterministic dynamics.

4.4 Perturbation analysis of the linear voter point

The other interesting (α_1, α_2) combination is the linear voter point $(0.2, 0.4)$ where *all* different regions of the mean-field phase diagram, Figure 3, intersect. Inserting $(0.2, 0.4)$ into equation (35) yields $dx/dt = 0$ regardless of the value of x, i.e. $x(t) = x(t = 0)$ for *all* initial conditions. This important feature of the linear VM was already discussed in Section 2.2. We recall that, while on the one hand the microscopic realizations always reach consensus (complete invasion of one species) in the long term, on the other hand an averaged outcome over many realizations shows that the share of the winning species is distributed as $x(t = 0)$. To put it the other way round, the mean-field limit discussed failes here because it does not give us any indication of the fact that there is a completely ordered state in the linear VM. The averaged outcome, for example $x = 0.5$, can result both from complete *invasion* of species 1 (50 *coexistence* of the two species). Both of these outcomes exist in the immediate neighborhood of the linear voter point as Figure 3 shows. In order to get more insight into this, we will later use the pair approximation derived in Section 3.3. Here, we first follow a perturbation approach, i.e. we add a small perturbation to the solution describing the macroscopic ordered state of complete invasion (consensus). In terms of the nonlinear response function $\kappa(f)$, expressed by the α_n in equation (33), this means a nonzero value of $\alpha_0 = \varepsilon$, i.e. a small parameter indicating the perturbation. With this, we arrive at a modified mean-field equation:

$$\frac{dx_p}{dt} = \varepsilon\Big[(1-x)^5 - x^5\Big] + \frac{dx}{dt} \tag{37}$$

where dx/dt is given by the nonperturbated mean-field equation (35) and the index p shall indicate the presence of the perturbation ε. Consequently, this changes both the value of the fixed points, previously given by equation (36) and their stability. Instead of a complete analysis in the $(\varepsilon, \alpha_1, \alpha_2)$ parameter state, we restrict the investigations to the vicinity of the linear voter point $(\alpha_1, \alpha_2) = (0.2, 0.4)$ where $dx/dt = 0$. Equation (37) then returns only one real stationary solution, $x_p^{stat} = 0.5$, which is independent of ε and stable. Consequently, any finite perturbation will destroy the characteristic feature of reaching an ordered state in the linear VM, i.e. complete invasion, and leaves only *coexistence* of both species as a possible outcome. This is little surpising because adding an $\alpha_0 > 0$ to the dynamics transforms the former attractor $x \to 0, 1$ into a repellor, i.e. it prevents reaching the ordered state. More interesting the question is, how the perturbated linear voter dynamics looks in detail. This is investigated in the next section by means of computer simulation, and in Section 5.1 by means of the pair approximation approach.

4.5 Computer simulations of the perturbated CA

For further insight into the dynamics of the nonlinear VM, we perform some computer simulations using the CA approach already described in Section 4.3. Is important to

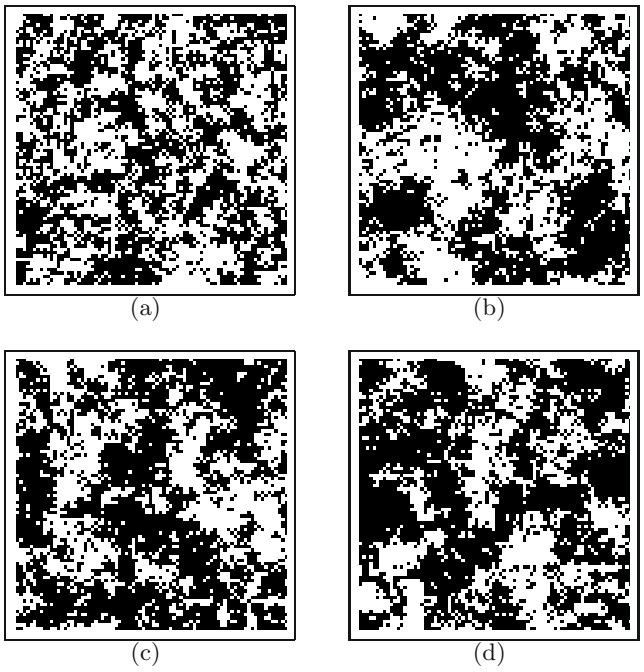

Fig. 6. Spatial snapshots of a positive frequency dependent invasion process with $\alpha_1 = 0.24$, $\alpha_2 = 0.30$, $\varepsilon = 10^{-4}$ (non-stationary, correlated coexistence). (a) $t = 10^1$, (b) $t = 10^2$, (c) $t = 10^3$, (d) $t = 10^4$. Note that a simulation using the parameters of the linear VM, $\alpha_1 = 0.2$, $\alpha_2 = 0.4$, would look statistically similar, and also the fluctuations of the global frequencies shown in Figure 7 are quite similar.

notice that we have chosen different sets of the parameters α_1, α_2 from the region of *positive frequency dependence*, as defined in Figure 2. I.e., the transition towards the opposite state strictly increases with the number of neighbors in that state (*majority voting*). So one would naively expect a similar macroscopic dynamics in that region as done in [29] This however is not the case as the following simulations indicate. A thorough analysis is presented in Section 5.2

In order to study the stability of the global dynamics for the different α_1, α_2 settings in the vicinity of the linear voter point, we have added a small perturbation $\alpha_0 = \varepsilon$. As the investigations of Section 4.4 have indicated, we should no longer expect consensus for the perturbated linear VM, but some sort of coexistence. In fact, we observe an interesting nonstationary pattern formation we call *correlated coexistence*. Figure 6 (obtained for another range of parameters α_1, α_2) shows an example of this. We find a long-term coexistence of both species, which is accompanied by a spatial structure formation. Here, the spatial pattern remains always nonstationary and the global frequency randomly fluctuates around a mean value of $x = 0.5$, as shown by Figure 7.

In more specific terms, the regime defined as 'correlated coexistence' is a paramagnetic phase with finite domain length, typical of partially phase-separated systems. We mention that such a regime was also observed in some

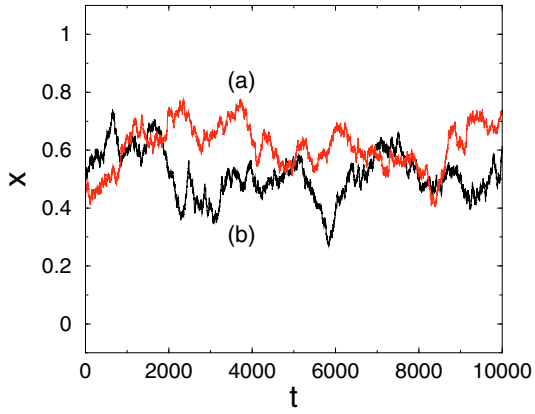

Fig. 7. Global frequency of species 1 vs. time (a) for the linear voter model, $\alpha_1 = 0.2$, $\alpha_2 = 0.4$, $\varepsilon = 10^{-4}$, and (b) for the same setup and parameters as in Figure 6. The initial frequency is $x(t = 0) = 0.5$ for both runs.

related investigations of the VM and other nonlinear spin models with Ising behavior [15,16]. Also, a similar transition was observed in the Abrams-Strogatz model [1], where the transition rate is a power a of the local field. The stability of the solutions then changes at $a = 1$, from coexistence for $a < 1$ to dominance for $a > 1$.

In order to find out about the range of parameters in the nonlinear VM resulting in the quite interesting phenomenon of correlated coexistence, we have varied the parameters α_1, α_2 within the region of positive frequency dependence. Figure 6 actually shows results from a set picked from region (f) in Figure 3, where the mean-field analysis predicts an asymmetric coexistence of both species. Obviously, the nonstationarity results from the perturbation ε.

However, for other sets α_1, α_2 in the positive frequency dependence region the perturbation does *not prevent* the system from reaching a global ordered state, i.e. invasion of one species as Figure 8 verifies. This process is accompanied by a clustering process and eventually a segregation of both species indicated by the formation of spatial domains. Figure 9 depicts the evolution of the global frequency $x(t)$ of species 1 for different initial frequencies $x(t{=}0)$. In every case, one species becomes extinct. For $x(t{=}0) > 0.5$ species 1 is the most likely survivor, while for $x(t{=}0) < 0.5$ it is most likely to become extinct. For $x(t{=}0) = 0.5$, random events during the early stage decide about its outcome.

On the other hand, the perturbation also does *not induce* an ordered state as the random coexistence in Figure 10 shows, which was again obtained from parameter settings in the region of positive frequency dependence. So, we conclude that computer simulations of *positive* frequency dependent processes show three different dynamic regimes (dependent on the parameters α_1, α_2): (i) complete invasion; (ii) random coexistence; and (iii) correlated coexistence. While for (i) and (ii) the outcome is in line with the mean-field prediction shown in Figure 4, this does not immediately follows for (iii). So, we are left with the question whether the interesting phenomenon of correlated coexistence is just *because* of the perturbation of

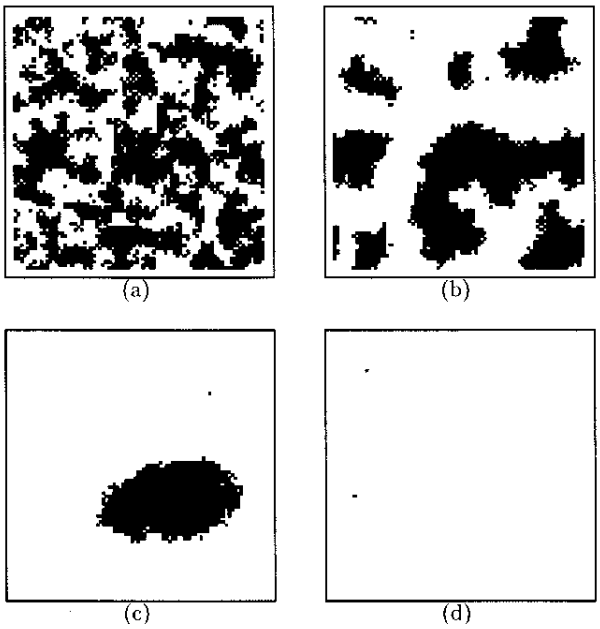

Fig. 8. Spatial snapshots of a positive frequency dependent invasion process with $\alpha_1 = 0.1$, $\alpha_2 = 0.3$, $\varepsilon = 10^{-4}$ (complete invasion). (a) $t = 10^1$, (b) $t = 10^2$ (c) $t = 10^3$, (d) $t = 10^4$.

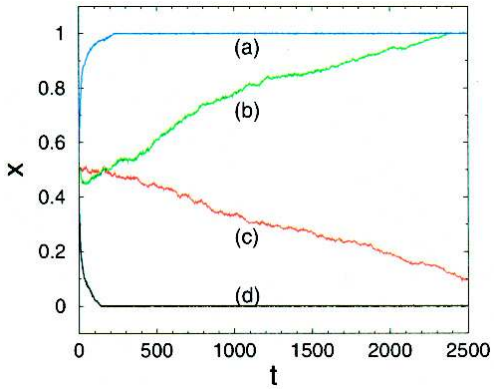

Fig. 9. Global frequency of species 1 vs. time for the same setup and parameters as in Figure 8. The initial frequencies $x(t = 0)$ of the four different runs are: (a) 0.6, (b) 0.5, (c) 0.5, (d) 0.4.

some ordered state, or whether it may also exist *inspite* of ε.

We just add that for *negative* frequency dependent invasion, equation (34), the the spatial pattern remains random, similar to Figure 10. Furthermore, regardless of the initial frequency $x(t=0)$, on a very short time scales, a global frequency $x^{\text{stat}} = 0.5$ is always reached. That means we always find *coexistence* between both species. We conclude that for *negative* frequency dependence $x^{\text{stat}} = 0.5$ is the only stable value, which is in agreement with the mean-field prediction, whereas for *positive* frequency dependence the situation is not as clear.

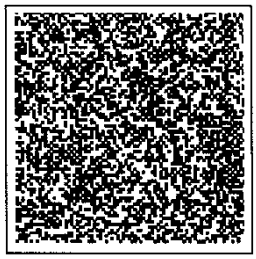

Fig. 10. Spatial snapshots of a positive frequency dependent invasion process with $\alpha_1 = 0.3$, $\alpha_2 = 0.4$, $\varepsilon = 10^{-4}$ (random coexistence). The snapshot shown at $t = 10^5$ is statistically equivalent to the initial random state.

5 Derivation of a phase diagram

To answer the question what ranges of α_1, α_2 eventually lead to what kind of macroscopic dynamics, we now make use of the pair approximation already derived in Section 3.3 as a first correction to the mean-field limit. Here, we follow a two-step strategy: first, we investigate how well the pair approximation, equations (38), (43), (44) of the macroscopic dynamics, equation (23), predict the global quantities $\langle x \rangle$ and $c_{1|1}$. In order to specify the network topology, we use again the CA described above. Second, we use the pair approximation to derive a phase diagram in the case of local interaction. Eventually, we test whether these findings remain stable against perturbations of the ordered state. All predictions are tested by comparison with computer simulations of the microscopic model, from which we calculate the quantities of interest and average them over 50 runs.

5.1 Global frequencies and spatial correlations

Here we have to distinguish between the three different dynamic regimes already indicated in Section 4.5.

Regime (i), *complete invasion*, is characterized by fixed points of the macroscopic dynamics of either $\{\langle x \rangle, c_{1|1}\} = \{1, 1\}$ or $\{\langle x \rangle, c_{1|1}\} = \{0, 0\}$. The CA simulations as well as also the pair approximation of the dynamics quickly converge to one of these attractors, dependent on the initial conditions.

Regime (ii), *random coexistence*, has only one fixed point, $\{\langle x \rangle, c_{1|1}\} = \{0.5, 0.5\}$, to which the CA simulations quickly converge. The pair approximation converges to $\langle x \rangle = 0.5$ after some initial deviations from the CA simulation, i.e. it relaxes on a different time scale ($t > 40$), but is correct in the long run. The approximation of the local correlation $c_{1|1}$ shows some deviations from the predicted value, $c_{1|1} = 0.5$. We have tested the case of random coexistence for various parameter values and found values for $c_{1|1}$ between 0.4 and 0.6. The discrepancy is understandable, since in the case of long-term coexistence some of the spatial patterns flip between two different random configurations with high frequency. Thus, while the global frequency settles down to 0.5, the microscopic dynamics is still nonstationary.

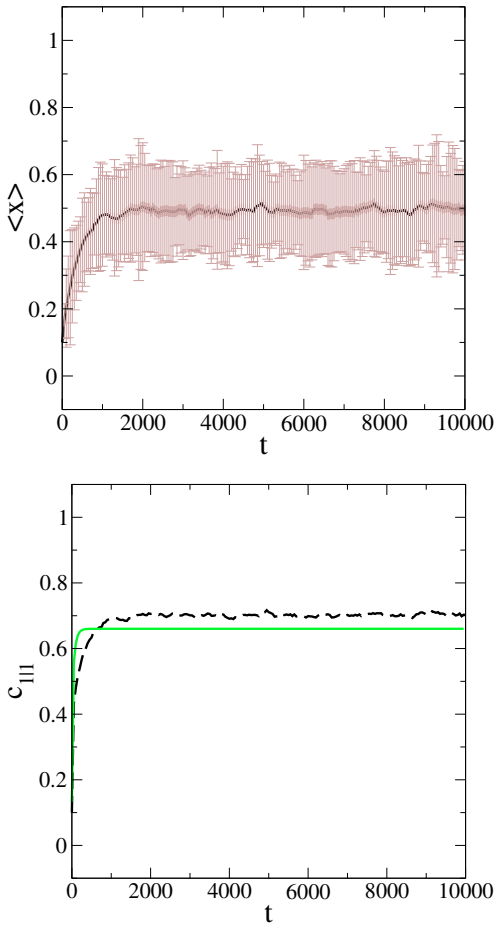

Fig. 11. Global frequency $\langle x \rangle$ with min-max deviations (top) and spatial correlation $c_{1|1}$ (bottom) for the case of correlated coexistence. The two curves shown in the bottom part result from averaging over 50 CA simulations (black dotted line) and from the pair approximation (green solid line). The parameters are as in Figures 6, 7 (top).

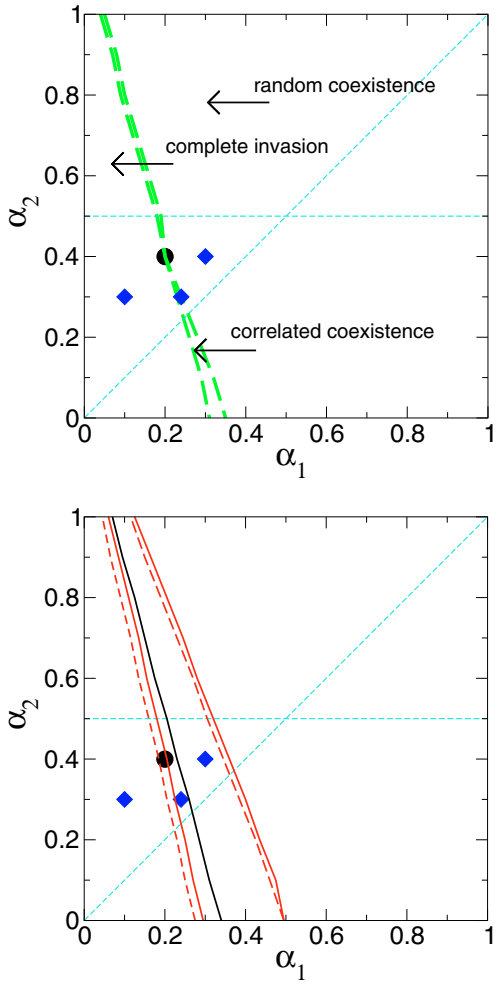

Fig. 12. Phase diagram of the nonlinear voter model: (top) CA simulations, averaged over 50 runs ($c_{1|1} = 0.7$), (bottom) pair approximation. Phase boundaries for $\varepsilon = 0$ resulting from $c_{1|1} = 0.65$ (upper limit): left – red solid line, right – black solid line, for comparison phase boundaries resulting from $c_{1|1} = 0.60$ (lower limit): left – red solid line (identical with $c_{1|1} = 0.65$), right – red solid line on the far right. Dashed red lines indicate the shift of the phase boundaries for $c_{1|1} = 0.60$ if $\varepsilon = 0.02$. The linear voter point (0.2, 0.4) is indicated by •. Further, ◇ marks those three parameter sets from the positive frequency dependence region where CA simulations are shown in Figures 8, 6, 10 (see also global frequency $\langle x \rangle$ and local correlation $c_{1|1}$ in Figs. 7, 9, 11). The straight dashed lines mark the different parameter areas given in equation (34) which are also shown in Figure 2.

Regime (iii), *correlated coexistence*, the most interesting one, is chacterized by an average global frequency of $\langle x \rangle = 0.5$ again, however the existing local correlations lead to a much higher value of $c_{1|1} > 0.6$. This is shown in Figure 11, where we find $c_{1|1} \approx 0.7$ from the CA simulations and $c_{1|1} \approx 0.65$ from the pair approximation. I.e., for the case of spatial domain formation the long-range correlations can be well captured by the pair approximation, whereas this was less satisfactory for the short-range correlations of the random patterns.

5.2 Determining the phase boundary

The insights into the dynamics of the nonlinear VM derived in this paper are now summarized in a phase diagram that identifies the different parameter regions (α_1, α_2) for the possible dynamic regimes identified in the previous sections. In order to find the boundaries between these different regimes, we carried out CA simulations of the complete parameter space, $0 \leq (\alpha_1, \alpha_2) \leq 1$. Precisely, for every single run the long-term stationary values of x and $c_{1|1}$ were obtained and then averaged over 50 simulations. As described above, the three different regimes could be clearly separated by their $\{\langle x \rangle, c_{1|1}\}$ values, which were used to identify the phase boundary between the different regimes. The outcome of the CA simulations is shown in the phase diagram of Figure 12 (top) and should be compared with Figure 3, which results from the mean-field analysis in Section 3.3 and thus neglects any kind of correlation.

Instead of the six regions distinguished in Figure 3, in the local case we can distinguish *two* different regions divided by one separatrix: the parameter region left of the separatrix refers to the *complete invasion* of one of the species, with *high* local correlations during the evolution. In the CA simulations, we observe the formation of domains that grow in the course of time until exclusive domination prevails. Asymptotically, a *stationary* pattern is observed, with $\langle x\rangle = 1$ (or 0) and $c_{1|1} = 1$ (or 0) (cf. the simulation results show in Figs. 8, 9). I.e., the system converges into a 'frozen' state with no dynamics at all. The region to the right of the separatrix refers to *random coexistence* of both species with $\langle x\rangle = 0.5$ and *no* local correlations, i.e. $c_{1|1} = 0.5$. In the CA simulations, we observe *nonstationary* random patterns that change with high frequency (cf. Fig. 10).

Both regions are divided by a *separatrix*. As shown in Figure 12 (top), the separatrix is divided into two pieces by the linear voter point, (0.2, 0.4). Above that point, the separatrix is very narrow, but below the voter point it has in fact a certain extension in the parameter space. Looking at the dynamics *on* the separatrix, we find that the mean frequency is $\langle x\rangle = 0.5$ both above and below the voter point (see also Fig. 11, top). The local correlation $c_{1|1} = 0.7$ holds within the whole extended area of the separatrix which identifies it as the region of *correlated coexistence* (see also Fig. 11, bottom).

The question is how well this phase diagram can be predicted by using the pair approximation of the dynamics, described by equations (38), (44). For a comparison, the coupled equations were numerically solved to get the asymptotic solutions for $\{\langle x\rangle, c_{1|1}\}$ (which looks complicated but is numerically very fast and efficient). In order to distinguish between the three regimes, we have to define a critical $c_{1|1}$ value for the correlations. Whereas in the CA simulations $c_{1|1} = 0.7$ indicated a correlated nonstationary coexistence, this value was never reached using the pair approximation (see Fig. 11, bottom), so $c_{1|1} \leq 0.65$ could be regarded as an *upper limit* for the case of correlated coexistence. Random coexistence, on the other end, yielded $c_{1|1} = 0.5$ in the CA simulations and a value between 0.4 and 0.6 in the pair approximation. So, given suitable initial conditions, we can regard $c_{1|1} \geq 0.6$ as a *lower limit*, to identify correlated coexistence. The results are shown in Figure 12 (bottom) which shall be compared with the phase diagram above (Fig. 12, top).

Figure 12 (bottom) shows the influence of the $c_{1|1}$ threshold value. With the lower limit, we find a quite broad region of correlated coexistence, which for example also includes the point $(0.3, 0.4)$ for which a random coexistence in the CA simulations was shown in Figure 10. Using the upper limit $c_{1|1} = 0.65$ results in a much smaller region of correlated coexistence. Comparing this with the CA simulations above, we can verify that the pair approximation correctly predicts the extended region below the voter point and also shows how it becomes more narrow above the voter point. One should note that the left border of the separatrics is not affected by the threshold value, whereas the right border shifts considerably. The left border also contains the voter point (independent of the $c_{1|1}$ threshold value), for which a complete invasion can be observed.

Therefore, it is quite interesting to look into changes of the phase diagram if additional perturbations are considered (see also Sect. 4.4). Figure 12 (bottom) shows (for the threshold $c_{1|1} = 0.6$) that this does *not* affects the existence of the three dynamic regimes and most notably of the extended separatrix below the voter point, but only shifts the boundaries toward the left, dependent on the value of $\alpha_0 = \varepsilon$ (this can be also verified for $c_{1|1} = 0.65$ but is omitted here, to keep the figure readable). Thus, the consideration of perturbations in the phase diagram reveals that it is indeed the *nonlinearity* in the voter model which allows for the interesting phenomenon of the correlated coexistence and *not* just the perturbation.

A closer look into Figure 12 (bottom) also shows that in the perturbated phase diagram the voter point no longer lies on the boundary towards the region of complete invasion but clearly *within* the region of correlated coexististence. This is in agreement with the findings in Section 4.4 which showed that for the linear VM complete invasion is an unstable phenomenon and changes into correlated coexistence for finite ε.

6 Discussion and conclusions

In this paper, we investigated a local model of frequency dependent processes, which for example models the dynamics of two species $\{0, 1\}$ in a spatial environment. Individuals of these species (also called 'voters') are seen as nodes of a network assumed as homogeneous in this paper (i.e. all nodes have the same number of neighbors, m). The basic assumption for the microscopic dynamics is that the probability to occupy a given node with either species 0 or 1 depends on the frequency of this species in the immediate neighborhood. Different from other investigations, we have counted in the state of the center node as well (see Sect. 2.2) and have further considered a *nonlinear response* of the voters to the local frequencies.

Studies of a nonlinear version of the traditional voter model (without counting the state of the central node and with sequential dynamics) have already been analyzed before. Reference [29], as pointed out before, is closest to our investigations, but restricted itself to the mean-field analysis and computer simulations of the $2d$ case, to obtain a phase diagram similar to Figure 12 (top). [31], on the other hand, have provided a Markov analysis which is restricted only to very small CA. The two-parameter model in [15] is for $y = 1$ a nonlinear voter model that exhibits at the voter point ($x = 1/2$) a transition from a ferromagnetic phase, i.e. invasion, for $x > 1/2$ to a paramagnetic phase (correlated coexistence) for $x < 1/2$. Also the case of the 'perturbated linear voter model' is included in the model, for $x = 1/2$ and $y < 1$. Similar results are also presented in [17], which points out relations to random branching processes, and in [11], where the emphasis is on investigations of the interface density, to describe the

coarsening process. A recent paper [51] also shows for spin systems with two symmetric absorbing states (such as the VM) that the macroscopic dynamics only depends on the first derivatives of the spin-flip probabilities.

In our paper, we set out for a formal approach that allows to derive the dynamics on different levels: (i) a *stochastic dynamics* on the microlevel, which is used for reference computer simulations but also allows a derivation of the (ii) *macroscopic dynamics* for the key variables, given in terms of differential equations. This macroscopic dynamics is then analysed by two different approximations, (i) a *mean-field approximation* that neglects any local interaction in the network, and (ii) a *local approximation* considering correlations between pairs of nearest neighbors. In order to test the validity of these approximations, we compare their predictions with the averaged outcome of the microscopic computer simulations. We like to emphasize that our approach is general enough to be applied to various forms of *frequency dependent processes* on homogeneous networks with different number of neighbors. Even if a two-dimensional regular lattice is used to illustrate the dynamics, the approach is not restricted to that.

Our main result, in addition to the general framework for nonlinear frequency dependent processes, is the derivation of a *phase diagram* using the *pair approximation* derived in this paper. This approach predicts correctly both the type of the dynamics and the asymptotic values of the key variables dependent on the possible nonlinearities for the case of *local interaction*, $m = 4$. The predicted phase diagram was verified by comparison with extensive microscopic computer simulations rastering the whole parameter space. While the structure of the phase diagram was already known from previous computer simulations presented in [29] we could demonstrate that the pair approximation works very well both for predicting the correct phase boundaries and the dynamics within these phases. It should be noticed that the pair approximation is a valuable tool, particularly with respect to computational efforts. The computer simulations are much more timeconsuming, since the results of the different runs have to be averaged afterwards. The pair approximation, on the other hand, is based on only 2 coupled equations and therefore needs less computational effort. In the following, we discuss some of the interesting findings.

The region of correlated coexistence: analysing the nonlinear VM with *local interaction* has shown that there are in fact only *three* different dynamic regimes dependent on the nonlinearities (α_1, α_2): (i) complete invasion, (ii) random coexistence, and (iii) correlated coexistence. The first one is already known as the standard behavior of the *linear* VM. Consequently the only interesting feature, namely the time to reach the ordered state dependent on the network size and topology, has been the subject of many investigations [9,47,48]. Number (ii), on the other hand, only leads to trivial results as no real dynamics is observed. Thus, the most interesting regime is (iii) correlated coexistence, which can be found in a small, but not negligible parameter region below the voter point. This region separates the two dominant regimes (i) and (ii) and therefore was called a separatrix here. Going over from the right to the left side of the phase diagram in that region, we notice a transition from 0.5 to 1.0 (or 0.0 respectively) in the mean frequency, and from 0.5 to 0.7 to 1.0 in the local correlations. Thus, in fact $c_{1|1}$ separates the two dynamic regimes (i) and (ii) (below the voter point). For parameters chosen from that region, we find in the CA simulations a long-term and nonstationary *coexistence* between the two species as on the *right* side of the phase diagram. But we also find the long-range spatial correlations that lead to the formation of spatial domains as shown e.g. in Figure 6 – which is characteristic for the *left* side of the phase diagram. The spatial pattern formation is also indicated by large fluctuations of $\langle x \rangle$ shown in Figure 11 (top). A single run, as shown in Figure 7, clearly indicates the long-term nonstationary coexistence of both species.

We emphasize that the separatrix between the two dynamic regimes is well predicted by the macroscopic dynamics resulting from the pair approximation (as can be clearly seen in Fig. 12). Most importantly, we could verify that the correlated coexistence of both species is not simply the effect of an additional perturbation, but results from the nonlinear interaction.

Comparison with the mean-field phase diagram: in our paper, the mean-field approximation plays the role of a reference state used to demonstrate the differences of the local analysis. The phase diagram of Figure 3 distinguishes between six different regions, whereas the one in the local case, Figure 12 (top) shows only three. Comparing the two phase diagrams, we realize that the most interesting regions in Figure 3, namely (c) and (f), have simply collapsed into the separatrix shown in Figure 12. The region (c) of unstable asymmetric coexistence or multiple outcome, respectively (see Sect. 4.2), relates to the separatrix line above the voter point. It should be noticed that the phase diagram for local interaction, Figure 12, correctly predicts that the deterministic behavior for $(\alpha_1, \alpha_2) = (0, 1)$ leads to complete invasion (see Sect. 5.2 and Fig. 5a).

The region (f) of stable asymmetric coexistence relates to the extended area of the separatrix shown below the voter point in Figure 12, where we still see a coexistence of both species – but the asymmetry between the two species relates to their changing dominance over time, as Figures 7, 11 (top) clearly illustrate. We conclude that in the local case no regions of stationary *and* asymmetric coexistence between the two species exist, as was predicted by the mean-field analysis. However, we find a (small but extended) region *on* the separatrix that shows the *nonstationary* and asymmetric coexistence of the two species for *single* realizations (which results in a symmetric coexistence averaged over runs, $\langle x \rangle = 0.5$, see Fig. 11, top).

The role of positive frequency dependence: the possible nonlinear responses in frequency dependent processes can be distinguished in four parameter areas of positive and negative frequency dependence and positive and negative allee effects, as Figure 2 shows. Previous investigations [29] assigned a dynamic leading to invasion to a

positive frequency dependence, while associating a spatial coexistence with negative frequency dependence. Our investigations have shown that such an assignment does not unambiguously hold. In particular, a random coexistence can be found for *negative* frequency dependent dynamics as well as for *positive* frequency dependence, which was so far assigned to complete invasion only [29]. On the other hand, complete invasion is not observed only for positive frequency dependence, but also for positive and negative allee effects. A random spatial coexistence can be found for positive and negative allee dynamics as well. The only case where just one dynamic regime can be observed is the case of negative frequency dependence. We note, however, that the nonstationary long-term coexistence with spatial pattern formation occurs both for the positive frequency dependence and the negative allee dynamics, given that the parameters are chosen from the most interesting zone of the separatrix below the voter point.

In conclusion, the region of positive frequency dependence bears in fact a much more richer dynamics, as it is transected by the separatrix we identified in the local analysis and thus shows all three types of dynamics we could identify for nonlinear voter models, namely (i) complete invasion of one of the species via the formation of large domains; (ii) long-term coexistence of both species with random distribution; (iii) long-term coexistence of both species with formation of nonstationary domains. However, the most interesting regime (iii) is *not* restricted to positive frequency dependent processes, but can be also found for some negative allee effects.

We summarize our findings by pointing out that *nonlinear* VM show indeed a very rich dynamics which was not much investigated yet. In addition to the phenomenon of complete invasion (or consensus) which occurs also beyond the linear VM, we find most interesting that certain parameter settings lead to a dynamics with nonstationarity and long-term correlations. Thinking about possible applications of the VM, we see that in particular this region has the potential to model relevant observations, be it the temporal dominance of certain species in a habitat or the temporal prevalence of certain opinions (or political parties) in a social system. The nonstationarity observed gives rise to the prediction that such dominance may not be the end, and change happens (even without additional perturbation).

The authors want to thank Thilo Mahnig and Heinz Mühlenbein for discussions on an early version of this paper.

Appendix

Here we derive some explicit expressions for the three equations of the pair approximation discussed in Section 3.3, for the global frequency $\langle x\rangle$ (Eq. (31)), the doublet frequency $\langle x_{1,1}\rangle$ and the correlation term $c_{1|1}$, equation (32). The equations are derived for the neighborhood $m = 4$. We use the notation $x \equiv \langle x\rangle$. Using equation (29) and the transition rates of equation (33), we find for $\langle x\rangle$, equation (31) in pair approximation:

$$\begin{aligned}\frac{dx}{dt} = \varepsilon\Big[&\frac{1}{(1-x)^3}(1-2x+xc_{1|1})^4 - x{c_{1|1}}^4\Big]\\ &+ 4\alpha_1\left[\frac{x}{(1-x)^3}(1-2x+xc_{1|1})^3(1-c_{1|1})\right.\\ &\left.- x(1-c_{1|1}){c_{1|1}}^3\right] + 6\alpha_2\left[\frac{x^2}{(1-x)^3}(1-2x\right.\\ &\left.+ xc_{1|1})^2(1-c_{1|1})^2 - x(1-c_{1|1})^2{c_{1|1}}^2\right]\\ &+ (1-\alpha_1)\left[\frac{x^4}{(1-x)^3}(1-c_{1|1})^4 - x(1-c_{1|1})^4\right]\\ &+ 4(1-\alpha_2)\left[\frac{x^3}{(1-x)^3}(1-2x+xc_{1|1})(1-c_{1|1})^3\right.\\ &\left.- x(1-c_{1|1})^3c_{1|1}\right]. \end{aligned} \tag{38}$$

We note that $c_{1|1} = c_{1|0} = x$ and $c_{0|0} = c_{0|1} = 1 - x$ in the mean-field limit, in which case equation (38) reduces to equation (35).

In order to calculate the time derivative of the doublet frequency $\langle x_{1,1}\rangle$ we have to consider how it is affected by changes of σ in a specific occupation pattern of size $m = 4$, $\underline{\sigma}^0 = \{\sigma, \sigma_1, \sigma_2, \sigma_3, \sigma_4\}$, considering the σ_j as constant. Again, in a frequency dependent process it is assumed that the transition does not depend on the exact distribution of the σ_j, but only on the frequency of a particular state σ in the neighborhood. Let $S_{\sigma,q}$ describe a neighborhood where the center node in state σ is surrounded by q nodes of the same state σ. For any given $q \leq m$, there are $\binom{m}{q}$ such occupation patterns. The global frequency of neighborhood $S_{\sigma,q}$ is denoted as $x_{\sigma,q}$ with the expectation value $\langle x_{\sigma,q}\rangle$. Obviously, $x_{\sigma,q}$ can be calculated from the global frequencies $x_{\sigma,\underline{\sigma}'}$ of all possible occupation distributions $\underline{\sigma}'$ (Eq. (3)), that match the condition

$$z^\sigma = \sum_{j=1}^{m} \delta_{\sigma,\sigma_j} \;:=\; q \tag{39}$$

i.e. it is defined as

$$x_{\sigma,q} = \sum_{\underline{\sigma}', z^{\sigma'}=q} x_{\sigma,\underline{\sigma}'}. \tag{40}$$

Regarding the possible transitions, we are only interested in changes of the doublet (1, 1), i.e. transitions $(1,1) \to (0,1)$ or $(0,1) \to (1,1)$. The transition rates shall be denoted as $w\big((0,1)|(1,1), S_{\sigma,q}\big)$ and $w\big((1,1)|(0,1), S_{\sigma,q}\big)$ respectively, which of course depend on the local neighborhood $S_{\sigma,q}$. With this, the dynamics of the expected doublet frequency can be described by the rate equation:

$$\begin{aligned}\frac{d}{dt}\langle x_{1,1}\rangle(t) = \sum_{q=0}^{m}\Big[&w\big((1,1)|(0,1), S_{0,q}\big)\langle x_{0,q}\rangle\\ &- w\big((0,1)|(1,1), S_{1,q}\big)\langle x_{1,q}\rangle\Big]. \end{aligned} \tag{41}$$

In order to specify the transition rates of the doublets $w\big((\sigma',1)|(\sigma,1),S_{\sigma,q}\big)$, with $\sigma'=1-\sigma$ and $\sigma\in\{0,1\}$, we note that there are only 10 distinct configurations of the neighborhood. Let us take the example $\underline{\sigma}^0=\{1,1,1,1,1\}$. A transition $1\to 0$ of the center node would lead to the extinction of 4 doublets $(\sigma,\sigma_j)=(1,1)$. On the other hand, the transition rate of the center node is ε as known from equation (33). This would result in $w\big((0,1)|(1,1),S_{1,4}\big)\propto 4\varepsilon$. However, for a lattice of size N the number of doublets is $2N$, whereas there are exactly N neighborhoods $\underline{\sigma}^0$. Therefore, if we apply the transition rates of the single nodes, equation (33), to the transition of the doublets, their rates have to be scaled by 2. Similarly, if we take the example $\underline{\sigma}^0=\{0,1,1,1,0\}$, a transition of the center node $0\to 1$ would occur at the rate $1-\alpha_2$ and would create 3 new doublets. Applying the scaling factor of 2, we verify that $w\big((1,1)|(0,1),S_{0,1}\big)=3/2\,(1-\alpha_2)$. This way we can determine the other possible transition rates:

$$
\begin{aligned}
w\big((0,1)|(1,1),S_{1,4}\big) &= 2\varepsilon\\
w\big((0,1)|(1,1),S_{1,3}\big) &= \frac{3}{2}\alpha_1\\
w\big((0,1)|(1,1),S_{1,2}\big) &= \alpha_2\\
w\big((0,1)|(1,1),S_{1,1}\big) &= \frac{1}{2}(1-\alpha_2)\\
w\big((0,1)|(1,1),S_{1,0}\big) &= 0\\
w\big((1,1)|(0,1),S_{0,4}\big) &= 0\\
w\big((1,1)|(0,1),S_{0,3}\big) &= \frac{1}{2}\alpha_1\\
w\big((1,1)|(0,1),S_{0,2}\big) &= \alpha_2\\
w\big((1,1)|(0,1),S_{0,1}\big) &= \frac{3}{2}(1-\alpha_2)\\
w\big((1,1)|(0,1),S_{0,0}\big) &= 2(1-\alpha_1). \qquad (42)
\end{aligned}
$$

Note that two of the transition rates are zero, because the respective doublets (1, 1) or (0, 1) do not exist in the assumed neighborhood. Finally, we express the $\langle x_{\sigma,q}\rangle$ in equation (41) by the $\langle x_{\sigma,\underline{\sigma}'}\rangle$ of equation (40) and apply the pair approximation, equation (30), to the latter one. This way, we arrive at the dynamic equation for $\langle x_{1,1}\rangle$:

$$
\begin{aligned}
\frac{d\langle x_{1,1}\rangle}{dt} = &-2\varepsilon x {c_{1|1}}^4 + 2\alpha_1\left[\frac{x}{(1-x)^3}(1-x\right.\\
&\left.+xc_{1|1})^3(1-c_{1|1}) - 3x(1-c_{1|1}){c_{1|1}}^3\right]\\
&+6\alpha_2\left[\frac{x^2}{(1-x)^3}(1-x+xc_{1|1})^2(1-c_{1|1})^2c_{1|1}^2\right.\\
&\left.-x(1-c_{1|1})^2\right]+2(1-\alpha_1)\left[\frac{x^4}{(1-x)^3}\right.\\
&\left.\times(1-c_{1|1})^4 - x(1-c_{1|1})^3\right]\\
&+2(1-\alpha_2)\left[\frac{x^3}{(1-x)^3}3(1-2x+xc_{1|1})\right.\\
&\left.\times(1-c_{1|1})^3 - x(1-c_{1|1})^3c_{1|1}\right]. \qquad (43)
\end{aligned}
$$

The third equation, equation (32), for the correlation term $c_{1|1}$ can be obtained in explicte form by using equation (38) for $\langle x\rangle$ and equation (43) for $\langle x_{1,1}\rangle$:

$$
\begin{aligned}
\frac{dc_{1|1}}{dt} = &-\varepsilon\left(\frac{c_{1|1}}{x(1-x)^3}(1-2x+xc_{1|1})^4 + {c_{1|1}}^5 - 2{c_{1|1}}^4\right)\\
&+\alpha_1(1-c_{1|1})\Big[{c_{1|1}}^3(4c_{1|1}-6)\\
&-2\frac{1}{(1-x)^3}(1-x+xc_{1|1})^3(2c_{1|1}-1)\Big]\\
&+6\alpha_2(1-c_{1|1})^3\left[\frac{x}{(1-x)^3}(1-x+xc_{1|1})^2 - c_{1|1}\right]\\
&+(1-\alpha_1)(1-c_{1|1})^4\left[\frac{x^3}{(1-x)^3}(2-c_{1|1})+c_{1|1}\right]\\
&+(1-\alpha_2)(1-c_{1|1})^3\Big[2c_{1|1}(2c_{1|1}-1)\\
&+\frac{x^2}{(1-x)^3}(1-2x+xc_{1|1})(6-4c_{1|1})\Big]. \qquad (44)
\end{aligned}
$$

References

1. D. Abrams, S. Strogatz, Nature **424**, 900 (2003)
2. P.S. Albin, *The Analysis of Complex Socioeconomic Systems* (Lexington Books, London, 1975)
3. J. Antonovics, P. Kareiva, Philos. Trans. R. Soc. London B **319**, 601 (1988)
4. L. Behera, F. Schweitzer, Int. J. Mod. Phys. C **14**, 1331 (2003)
5. E. Ben-Naim, L. Frachebourg, P.L. Krapivsky, Phys. Rev. E **53**, 3078 (1996)
6. E. Ben-Naim, P. Krapivsky, S. Redner, Physica D: Nonlinear Phenomena **183**, 190 (2003)
7. A.T. Bernardes, D. Stauffer, J. Kertesz, Eur. Phys. J. B **25**, 123 (2002)
8. C. Castellano, S. Fortunato, V. Loreto, Rev. Mod. Phys. (2008) http://arxiv.org/abs/0710.3256
9. C. Castellano, V. Loreto, A. Barrat, F. Cecconi, D. Parisi, Phys. Rev. E **71**, 066107 (2005)
10. C. Castellano, D. Vilone, A. Vespignani, Europhys. Lett. **63**, 153 (2003)
11. X. Castello, V. Eguíluz, M. San Miguel, New J. Phys. **8**, 308 (2006)
12. R.N. Costa Filho, M.P. Almeida, J.S. Andrade, J.E. Moreira, Phys. Rev. E **60**, 1067 (1999)
13. J.T. Cox, D. Griffeath, Annals of Probability **14**, 347 (1986)
14. L. Dall'Asta, C. Castellano, Europhys. Lett. **77**, 60005 (2007)
15. M. De Oliveira, J. Mendes, M. Santos, J. Phys. A **26**, 2317 (1993)
16. I. Dornic, H. Chaté, J. Chave, H. Hinrichsen, Phys. Rev. Lett. **87**, 045701 (2001)

17. J. Drouffe, C. Godrèche, J. Phys. A: Mathematical and General **32**, 249 (1999)
18. R. Durrett, S. Levin, Theoretical Population Biology **46**, 363 (1994)
19. L. Frachebourg, P. Krapivsky, Phys. Rev. E **53**, R3009 (1996)
20. R.A. Holley, T.M. Liggett, Annals of Probability **3**, 643 (1975)
21. J. Hołyst, K. Kacperski, F. Schweitzer, Physica A **285**, 199 (2000)
22. T.H. Keitt, M.A. Lewis, R.D. Holt, The American Naturalist **157**, 203 (2001)
23. B.E. Kendall, O.N. Bjørnstad, J. Bascompte, T.H. Keitt, W.F. Fagan, The American Naturalist **155**, 628 (2000)
24. M. Kimura, G.H. Weiss, Genetics **49**, 313 (1964)
25. P. Krapivsky, Phys. Rev. A **45**, 1067 (1992)
26. P.L. Krapivsky, S. Redner, Phys. Rev. Lett. **90**, 238701 (2003)
27. T.M. Liggett, Annals of Probability **22**, 764 (1994)
28. T.M. Liggett, *Stochastic Interacting Systems*, *Grundlehren der mathematischen Wissenschaften* (Springer, Berlin, 1999), Vol. 342
29. J. Molofsky, R. Durrett, J. Dushoff, D. Griffeath, S. Levin, Theoretical Population Biology **55**, 270 (1999)
30. C. Moore, J. Stat. Phys. **88**, 795 (1997)
31. H. Mühlenbein, R. Höns, Advances in Complex Systems **5**, 301 (2002)
32. M. Nakamaru, H. Matsuda, Y. Iwasa, J. Theor. Biology **184**, 65 (1997)
33. C. Neuhauser, Theoretical Population Biology **56**, 203 (1999)
34. A. Nowak, M. Kus, J. Urbaniak, T. Zarycki, Physica A **287**, 613 (2000)
35. N.A. Oomes, D. Griffeath, C. Moore, *New Constructions in cellular automata* (Oxford Universitiy Press, 2002), pp. 207–230
36. S.W. Pacala, J.A. Silander, Jr., The American Naturalist **125**, 385 (1985)
37. S. Redner, *A guide to first-passage processes* (Cambridge University Press, Cambridge, 2001)
38. F.J. Rohlf, G.D. Schnell, The American Naturalist **105**, 295 (1971)
39. T. Schelling, Am. Econ. Rev. **59**, 488 (1969)
40. F. Schweitzer, *Brownian Agents and Active Particles. Collective Dynamics in the Natural and Social Sciences*, Springer Series in Synergetics (Springer, Berlin, 2003)
41. F. Schweitzer, L. Behera, H. Mühlenbein, Advances in Complex Systems **5**, 269 (2002)
42. F. Schweitzer, J. Hołyst, Eur. Phys. J. B **15**, 723 (2000)
43. F. Slanina, H. Lavicka, Eur. Phys. J. B **35**, 279 (2003)
44. V. Sood, S. Redner, Phys. Rev. Lett. **94**, 178701 (2005)
45. H.-U. Stark, C.J. Tessone, F. Schweitzer, Phys. Rev. Lett. **101**, 018701 (2008)
46. H.-U. Stark, C.J. Tessone, F. Schweitzer, Advances in Complex Systems **11**, 87 (2008)
47. K. Suchecki, V.M. Eguíluz, M. San Miguel, Europhys. Lett. **69**, 228 (2005)
48. K. Suchecki, V.M. Eguíluz, M. San Miguel, Phys. Rev. E **72**, 036132 (2005)
49. G. Szabó, T. Antal, P. Szabó, M. Droz, Phys. Rev. E **62**, 1095 (2000)
50. F. Vazquez, V.M. Eguiluz, M.S. Miguel, Phys. Rev. Lett. **100**, 108702 (2008)
51. F. Vazquez, C. Lopez, Phys. Rev. E **78**, 061127 (2008)
52. W. Weidlich, J. Mathematical Sociology **18**, 267 (1994)